A Single Regrowth Integration Platform for Photonic Circuits Incorporating Tunable SGDBR Lasers and Quantum-Well EAMs

Matthew N. Sysak, *Member, IEEE*, James W. Raring, *Student Member, IEEE*, Jonathon S. Barton, *Member, IEEE*, Matthew Dummer, *Student Member, IEEE*, Daniel J. Blumenthal, *Fellow, IEEE*, and Larry A. Coldren, *Fellow, IEEE*

***Abstract*—A monolithic integration platform is demonstrated for high functionality photonic circuits that include quantum-well electroabsorption modulators, semiconductor optical amplifiers, and widely tunable lasers. The platform is based on the selective removal of a set of active quantum wells located above an optical waveguide layer. The waveguide layer contains a second set of quantum wells to be used in modulator regions. Fabrication requires only a single blanket InP regrowth.**

***Index Terms*—Electroabsorption modulators (EAMs), monolithic integration, quantum confined stark effect (QCSE), sampled grating distributed Bragg reflector (SGDBR) laser, semiconductor lasers, semiconductor optical amplifier (SOA).**

I. Introduction

THE development of high functionality photonic integrated circuits (PICs) is critical for reducing packaging costs and improving performance in next-generation networks. As a precursor to such devices, an integration platform must be available that requires simple fabrication and growth procedures in order to minimize processing requirements and maximize device yields. Several viable platforms have been demonstrated using the InGaAsP–InP material system. These include selective area growth, butt-joint regrowth, quantum-well intermixing, and offset quantum-well (OQW) platforms [1].

For PICs that require a tunable laser source integrated with electroabsorption modulators (EAMs) and semiconductor optical amplifiers (SOAs), the OQW platform employing sampled grating distributed Bragg reflector (SGDBR) lasers has been shown to be one of the simplest solutions [2]. A diagram of the layer structure in this platform is shown in Fig. 1(a). In this approach, quantum wells (QWs) located above a bulk InGaAsP waveguide layer are used for optical gain. To define regions where gain is not necessary, a wet selective etch is performed to remove these QWs. The etch terminates on a 15-nm InP regrowth and stop etch (SE) layer. To form the top p-contact, a blanket Zn-doped p-InP and p-InGaAs regrowth is performed. EAMs are defined by contacting and reverse biasing passive waveguide sections. Though very simple to implement, EAMs of this type are dependent on the Franz–Keldysh electroabsorption effect (FK-EAMs). This effect has limited modulation efficiency with low insertion loss, and exhibits positive chirp. In contrast, QW-EAMs employing the quantum confined stark effect (QCSE) have demonstrated large bandwidths, excellent modulation efficiency, low insertion loss, and negative chirp [3].

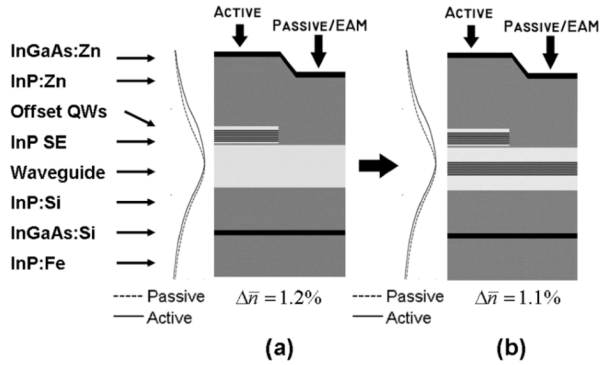

Fig. 1. Epitaxial layer structure and active/passive mode profiles for the (a) OQW and (b) DQW platforms. The modal effective index mismatch for transitions between active and passive regions is $<1.3\%$ for both approaches.

In this work, we present a newly developed dual-quantum-well (DQW) integration platform where the OQW approach is modified to obtain QCSE-based EAMs. A diagram of the DQW platform is shown in Fig. 1(b). In this new platform, the same selective etching and blanket regrowth techniques used in the OQW approach are employed to define optical gain (active) and passive/EAM regions. However, to enhance the EAM modulation efficiency, bandwidth, and chirp characteristics, a second set of QWs is placed into the center of the waveguide layer. The photoluminescence (PL) peak of the added wells is detuned from the offset QWs to balance propagation loss and laser performance with EAM efficiency.

To demonstrate the viability of the DQW platform, we have compared active region material characteristics and EAM performance for both the OQW and DQW platforms using a set of integrated widely tunable transmitters.

II. DQW Integration Platform

The offset QWs in the DQW platform are identical to those in the OQW approach. The offset QW stack consists of 7×6.5 nm compressively strained wells and 8×8.0 nm tensile strained barriers with a PL peak of 1550 nm. Below the offset wells is a 345-nm InGaAsP waveguide layer. In the center of the waveguide is the second set of QWs consisting of 7×9.0 nm compressively strained wells and 6×5.0 nm tensile strained barriers

Manuscript received March 2, 2006; revised April 20, 2006. This work was supported by the Defense Advanced Research Projects Agency (DARPA)/MTO CS-WDM under Grant N66001-02-C-8026 and by Intel Corporation under Grant TXA001630000.

The authors are with the Department of Electrical Engineering and the Department of Materials, University of California Santa Barbara, Santa Barbara, CA 93116 USA (e-mail: mnsysak@engineering.ucsb.edu).

Digital Object Identifier 10.1109/LPT.2006.878153

TABLE I
SUMMARY AND COMPARISON OF MATERIAL PARAMETERS

Platform	Injection efficiency (η_i)	Transparency current density (A/cm^2)	Material gain (cm^{-1})	Active loss (cm^{-1})
DQW	73 %	269.9	764	10
OQW	75 %	246	826.4	10

with a PL peak of 1480 nm. The conduction and valence band offsets for the waveguide QWs are 65 and 97 meV, respectively.

Above and below the waveguide QWs is a 25-nm undoped outer barrier layer. The remaining waveguide consists of high bandgap (1.3 μm) material that is lightly doped n-type (Si) at 5×10^{16} cm^{-3}. Since the waveguide doping levels are low, the electric field at the QWs with a reverse bias is almost identical to that in a standard PIN structure.

III. DQW PLATFORM MATERIAL PARAMETERS

When introducing a set of QWs into the waveguide layer, it is critical that the propagation loss and optical gain properties of the integrated SGDBR laser, optical amplifier, and passive waveguides are not degraded. Under forward bias operation, injected carriers must travel to the offset QWs without parasitic recombination for high laser injection efficiency. For holes, the transport path is identical to that in the OQW platform. Carriers are injected from p-cladding into the offset wells and trapped by the potential barrier created by the InP SE layer above the waveguide. The SE is thin enough to avoid vertical coupling effects in the active region, but maintain repeatability in the selective wet etch process. However, for electrons, carriers from the n-buffer layer must pass through the potential barriers associated with the waveguide QWs and over the InP SE layer before entering the OQWs for recombination.

To examine the carrier transport process in the DQW platform, pulsed differential efficiency measurements were performed on a set of 50-μm-wide Fabry–Pérot broad area lasers (BAL) and 3-μm-wide active ridge lasers (RLs) using the cleave back method. From the RLs, the injection efficiency and the modal active region propagation loss at 1550 nm was extracted. From the threshold current and differential efficiency of the BALs, a two parameter fit material gain curve was generated after accounting for the offset QW confinement factor of 6.2 %. These results are summarized in Table I and are in excellent agreement with measurements from devices fabricated on the OQW platform containing a moderately doped n-type (1.41-μm bandgap, 2×10^{17} cm^{-3} Si) waveguide. This indicates minimal or no added parasitic recombination in the waveguide QWs.

The other key material parameter that has been examined for the DQW integration platform is the passive region propagation loss over wavelengths within the telecommunications C-band. To investigate this, structures have been fabricated that contain a tunable laser source and a 3-mm-long passive waveguide. Electrical contacts are placed periodically along the passive waveguide and reverse biased to measure the photocurrent at each point along the structure. Based on the ratio of the photocurrents at each contact and the separation between pads, the propagation loss can be calculated. Results showed losses of 6 cm^{-1} at 1562 nm, 7.5 cm^{-1} at 1550 nm, 10 cm^{-1} at 1542 nm, and 16 cm^{-1} at 1530 nm. The exponential dependence of the propagation loss is expected based on an Urbach absorption tail resulting from the bandgap energy proximity between the waveguide and OQW stacks [4]. The propagation loss for the OQW waveguides was 6 cm^{-1} at 1550 nm. This is not expected to vary greatly due to the large bandgap detuning.

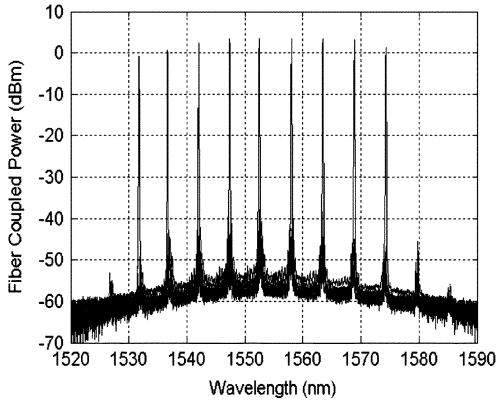

Fig. 2. Superimposed fiber coupled SGDBR spectra at various wavelengths. Laser gain and SOA postamplifier are biased at 100 mA.

IV. DQW TUNABLE TRANSMITTER

To demonstrate the viability of the DQW integration platform for use in high functionality PICs and to compare performance of the QW-EAMs with OQW FK-EAMs, we have fabricated a set of widely tunable transmitters. Devices consisted of a four-section SGDBR laser, a 400-μm-long SOA and a 400-μm-long EAM. To minimize parasitic capacitance, photo-bis-benzocyclobutene was used as a low-k dielectric. The separation between the SGDBR front mirror and SOA postamplifier is 50 μm, and between the SOA postamplifier and EAM is 100 μm. Device isolation is accomplished by selective removal of the Zn : InGaAs layer and a proton implant. All transmitters were antireflection-coated, soldered on AlN carriers, and wirebonded for characterization. The temperature in the following experiments was held at 17 °C.

For the DQW SGDBR, on-chip light versus current characteristics and fiber coupled output spectra at various wavelengths have been collected. The on-chip light output–current–voltage (L–I–V) data is extracted by reverse biasing the SOA that spatially follows the front mirror of the laser, and monitoring the detected photocurrent. The threshold current for the SGDBR was 38 mA at 1550 nm and optical power levels up to 12 mW were observed at a gain region bias current of 100 mA. Superimposed fiber coupled SGDBR spectra at various wavelengths are shown in Fig. 2 with both laser gain and SOA biased at 100 mA. Output powers ranged from 0 dBm at 1532 nm to 5 dBm at 1560 nm with fiber coupling losses measured at 4.5 dB. The sidemode suppression ratio for all operating wavelengths is greater than 30 dB.

The performance of the DQW EAMs and OQW EAMs (1.41-μm bandgap, 2×10^{17} cm^{-3} Si) were evaluated based on several device characteristics. These included measurements of the broadband dc extinction, small signal 50 Ω terminated S_{21} electrical to optical response, and the large signal chirp.

Normalized dc extinction measurements are shown in Fig. 3. At wavelengths of 1532, 1545, and 1560 nm, respectively,

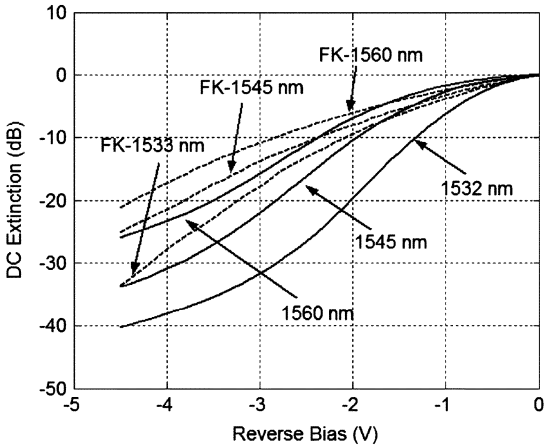

Fig. 3. Normalized dc extinction DQW (solid lines, 1532, 1545, and 1560 nm) and FK (dashed lines, 1533, 1545, 1560 nm) integrated EAMs.

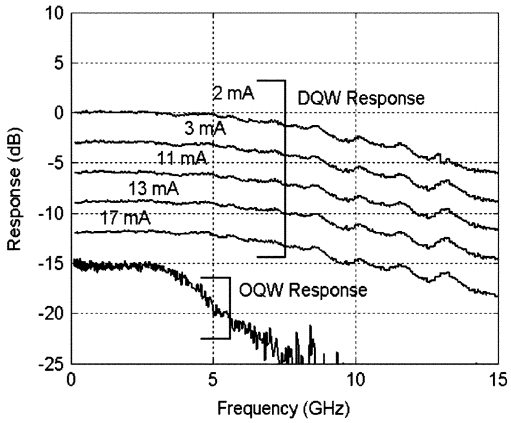

Fig. 4. S_{21} measurements for DQW and OQW EAMs. Data is spaced at 3-dB intervals for clarity Average waveguide photocurrent is indicated.

the DQW EAMs show modulation depths of −40, −33, and −26 dB, and peak modulation efficiencies of 16, 13, and 10 dB/V. Compared with FK-EAMs at similar wavelengths, this corresponds to improvements between 4 and 6 dB for the modulation depth and 4 and 3 dB/V for the modulation efficiency. The insertion loss of both EAM types is compared by combining the on-state insertion loss with the wavelength dependent propagation loss. The comparison is performed at dc bias points that maximize slope efficiency. For the QW-EAMs, the optimal slope efficiency at 1545 nm occurs at −2.4 V. With a 1-V pp modulation, the on-state loss from Fig. 3 is −5 dB. Combining this with the wavelength-dependent propagation loss for a 400-μm-long device, the total loss is −6.75 dB. A similar calculation for an FK-EAM operating at 1545 nm that has been biased for maximum slope efficiency (−4.5 V) gives a total EAM insertion loss of −18 dB.

Electrical-to-optical S_{21} measurements for OQW and DQW EAMs are shown in Fig. 4 at a bias of −3 V. The 3-dB bandwidth is improved from 4 to 10 GHz for the QW-EAMs. This result corresponds well with the larger depletion thickness that is expected using the lower waveguide doping employed in the DQW epitaxial structure. Since it is well known that

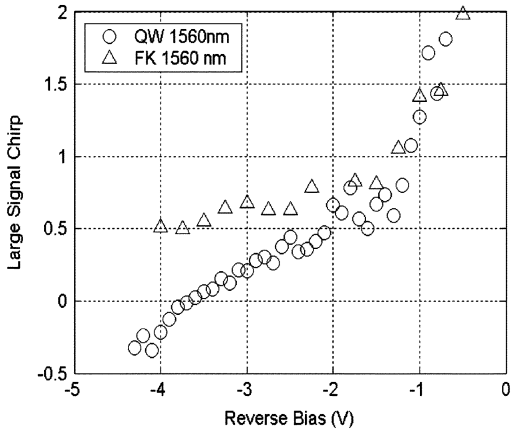

Fig. 5. The 10-Gb/s large signal time resolved chirp results at 1560 nm for integrated OQW FK-EAMs and DQW QW-EAMs under reverse bias.

QW-EAMs suffer from carrier screening effects, measurements on the DQW devices were performed for a variety of waveguide photocurrent levels. DQW EAMs show no deviation in bandwidth with up to 17 mA of photocurrent. Alternatively, similar FK-EAMs have been shown to be compatible with large optical power levels in [5].

The EAM chirp characteristics are shown in Fig. 5. This measurement was performed at 10 Gb/s using the Agilent Time Resolved Chirp (TRC) software with the SGDBR laser transmitters tuned to 1560 nm. This wavelength was selected because the large detuning between the laser wavelength and the waveguide absorption peak represents a condition where it is difficult to obtain small chirp values [3]. The DQW EAMs that employ the QCSE show lower chirp values at applied bias levels greater than −2 V, with zero chirp at −3.8 V.

V. Conclusion

We have demonstrated a DQW integration platform for advanced photonic circuits that requires a single blanket InP regrowth step to realize QW-EAMs, widely tunable lasers, and optical amplifiers. Integrated EAMs fabricated in this new platform show larger bandwidths, improved efficiency, lower insertion loss, and reduced chirp when compared with FK-EAMs that are available using a similar OQW platform.

References

[1] J. W. Raring, M. N. Sysak, A. Tauke-Pedretti, M. Dummer, E. J. Skogen, J. S. Barton, S. P. Senbaars, and L. A. Coldren, "Advanced integration schemes for high functionality/high performance photonic integrated circuits," in *Proc. Photonics West*, San Jose, CA, 2006.

[2] Y. A. Akulova, G. A. Fish, P. C. Koh, C. Schow, P. Kozodoy, A. Dahl, S. Nakagawa, M. Larsen, M. Mack, T. Strand, C. Coldren, E. Hegblom, S. Penniman, T. Wipiejewski, and L. A. Coldren, "Widely-tunable electroasbsorption-modulated sampled grating DBR laser transmitter," *IEEE J. Sel. Topics Quantum Electron.*, vol. 8, no. 6, pp. 1349–1357, Nov./Dec. 2002.

[3] G. L. Li and P. K. L. Yu, "Optical intensity modulators for digital and analog applications," *J. Lightw. Technol.*, vol. 21, no. 9, pp. 2010–2030, Sep. 2003.

[4] J. Dow and D. Redfield, "Toward a unified theory of Urbach's rule and exponential absorption edge," *Phys. Rev. B*, vol. 5, p. 594, Jan. 1972.

[5] L. A. Johansson, Y. A. Akulova, G. A. Fish, and L. A. Coldren, "High optical power electroabsorption modulator," *Electron. Lett.*, vol. 39, no. 4, pp. 364–365, Feb. 2003.